Absolute gas-phase acidities of CH_3NH_2, $C_2H_5NH_2$, $(CH_3)_2NH$, and $(CH_3)_3N$

GERVASE I. MACKAY,[1] RONALD S. HEMSWORTH,[2] AND DIETHARD K. BOHME[3]

Department of Chemistry, York University, Downsview, Ontario M3J 1P3

Received August 13, 1975

GERVASE I. MACKAY, RONALD S. HEMSWORTH, and DIETHARD K. BOHME. Can. J. Chem. **54**, 1624 (1976).

The flowing afterglow technique has been employed in measurements of the rate and equilibrium constants at 296 ± 2 K for reactions of the type

$$H^- + R_1R_2NH \rightleftarrows R_1R_2N^- + H_2$$

and

$$NH_2^- + R_1R_2NH \rightleftarrows R_1R_2N^- + NH_3$$

where R_1 and R_2 may be H, CH_3, or C_2H_5. The equilibrium constant measurements provided absolute values for the intrinsic (gas-phase) acidities of the Brønsted acids CH_3NH_2, $C_2H_5NH_2$, $(CH_3)_2NH$, and $(CH_3)_3N$, the heats of formation of their conjugate bases, and the electron affinities of the corresponding radicals R_1R_2N. Proton removal energies, ΔG^0_{298}/(kcal mol^{-1}), were determined to be 395.7 ± 0.7 for $CH_3NH_2 \rightleftarrows CH_3NH^- + H^+$, 391.7 ± 0.7 for $C_2H_5NH_2 \rightleftarrows C_2H_5NH^- + H^+$, 389.2 ± 0.6 for $(CH_3)_2NH \rightleftarrows (CH_3)_2N^- + H^+$, and >396 for $(CH_3)_3N \rightleftarrows (CH_3)_2NCH_2^- + H^+$. Heats of formation, $\Delta H^0_{f,298}$, were determined to be 30.5 ± 1.5 for CH_3NH^-, 21.2 ± 1.5 for $C_2H_5NH^-$, and 24.7 ± 1.4 for $(CH_3)_2N^-$. Electron affinities (in kcal mol^{-1}) were determined to be 13.1 ± 3.5 for CH_3NH, 17 ± 4 for C_2H_5NH, and 14.3 ± 3.4 for $(CH_3)_2N$. These results quantify earlier conclusions regarding the intrinsic effects of substituents on the gas-phase acidity of amines and provide an experimental assessment of recent molecular orbital calculations of proton removal energies for alkylamines.

GERVASE I. MACKAY, RONALD S. HEMSWORTH et DIETHARD K. BOHME. Can. J. Chem. **54**, 1624 (1976).

On a utilisé la technique de la lueur d'écoulement pour mesurer les vitesses et les constantes d'équilibres à 296 ± 2 K des réactions de type

$$H^- + R_1R_2NH \rightleftarrows R_1R_2N^- + H_2$$

et

$$NH_2^- + R_1R_2NH \rightleftarrows R_1R_2N^- + NH_3$$

où R_1 et R_2 peuvent être H, CH_3 ou C_2H_5. Les mesures des constantes d'équilibres fournissent des valeurs absolues pour les acidités intrinsèques (en phase gaseuse) des acides de Brønsted CH_3NH_2, $C_2H_5NH_2$, $(CH_3)_2NH$ et $(CH_3)_3N$ de même que les chaleurs de formation de leurs bases conjugées et les affinités électroniques des radicaux R_1R_2N correspondants. On a déterminé les énergies ΔG^0_{298}/(kcal mol^{-1}) nécessaires pour enlever les protons; les valeurs s'établissent à 395.7 ± 0.7 pour $CH_3NH_2 \rightleftarrows CH_3NH^- + H^+$, à 391.7 ± 0.7 pour $C_2H_5NH_2 \rightleftarrows C_2H_5NH^- + H^+$ à 389.2 ± 0.6 pour $(CH_3)_2NH \rightleftarrows (CH_3)_2N^- + H^+$ et à >396 pour $(CH_3)_3N \rightleftarrows (CH_3)_2NCH_2^- + H^+$. On a déterminé que les chaleurs de formation, $\Delta H^0_{f,298}$, sont 30.5 ± 1.5 pour CH_3NH^-, 21.2 ± 1.5 pour $C_2H_5NH^-$ et 24.7 ± 1.4 pour $(CH_3)_2N^-$. On a déterminé que les affinités électroniques (en kcal mol^{-1}) sont 13.1 ± 3.5 pour CH_3NH, 17 ± 4 pour C_2H_5NH et 14.3 ± 3.4 pour $(CH_3)_2N$. Ces résultats permettent d'établir d'une façon quantitative les conclusions antérieures se rapportant aux effets intrinsèques des substituants sur l'acidité en phase gaseuse des amines et fournissent une base expérimentale pour des calculs d'orbitales moléculaires récents concernant les énergies d'enlèvement de protons des alkylamines.

[Traduit par le journal]

Introduction

Recent developments in experimental techniques (1), *viz.* pulsed ion cyclotron resonance, pulsed electron beam high-pressure mass spec-

[1]This work was presented by G. I. Mackay in partial fulfilment of the Ph.D. requirements.

[2]Present address: Culham, UKAEA Research Group, Abingdon, Berkshire, England.

[3]Alfred P. Sloan Research Fellow, 1974–1976.

trometry, and the flowing afterglow technique, have provided a means of measuring, in the gas phase, rate and equilibrium constants for ion–molecule reactions of the type often encountered in solution. In the case of proton transfer reactions such measurements have proven to be useful for (*i*) the determination of intrinsic molecular properties of acids and their conjugate bases, (*ii*) the experimental assessment of molecular orbital calculations of such properties, and (*iii*) the thermodynamic analysis of the transfer of protonated species from the gas phase to solution. Aliphatic amines represent an important group of acids whose gas-phase acidities have recently been ordered (2) from determinations of the preferred direction of proton transfer reactions of the type

$$[1] \quad R_1R_2N^- + R_3R_4NH \rightleftarrows R_3R_4N^- + R_1R_2NH$$

In this paper we report flowing afterglow measurements of the rate and equilibrium constants at 296 ± 2 K for reactions of the type

$$[2] \quad NH_2^- + R_1R_2NH \rightleftarrows R_1R_2N^- + NH_3$$

$$[3] \quad H^- + R_1R_2NH \rightleftarrows R_1R_2N^- + H_2$$

where R_1 and R_2 may be H, CH_3, or C_2H_5. The equilibrium constant measurements provide absolute values for the intrinsic (gas-phase) acidities of the Brønsted acids CH_3NH_2, $C_2H_5NH_2$, $(CH_3)_2NH$, and $(CH_3)_3N$, the heats of formation of their conjugate bases, and the electron affinities of the corresponding radicals R_1R_2N. These results quantify earlier conclusions (based on measurements of orders of acidity) regarding the intrinsic effects of substituents on the gas-phase acidity of amines (2) and also provide an experimental assessment of recent molecular orbital calculations of proton removal energies for alkylamines (3–5).

Experimental

The experiments were performed with the flowing afterglow technique and are of the type described previously (6). Reactant ions are produced in a flowing plasma either by electron impact or by secondary ionization or ion–molecule reactions. In these experiments the plasma was generated with ionizing electrons having energies in the range 35–70 eV. The filament emission of the electron gun was 0.5 mA.

The neutral reactant is introduced sufficiently downstream of the ion production region to ensure that the reactant ions have undergone enough collisions with the carrier gas (helium was used in the experiments reported here) to become thermalized at the ambient room temperature (296 ± 2 K). The plasma communicates with a quadrupole mass spectrometer through a small orifice mounted at the tip of a sampling nose cone. Rate constants and equilibrium constants for reactions of ions with molecules are determined by measuring changes in ion signals as a function of the addition of neutral reactant molecules.

The gases used were He (Linde, Prepurified Grade, 99.995% He), NH_3 (Matheson, Anhydrous 99.99% min (liquid phase)), H_2 (Linde, Very Dry Grade 99.95% H_2), CH_3NH_2 (Matheson, 98.0% min (liquid phase)), $C_2H_5NH_2$ (Matheson, 98.5% min (liquid phase)), $(CH_3)_2NH$ (Matheson, 99.0% min (liquid phase)), and $(CH_3)_3N$ (Matheson, 99.0% min (liquid phase)).

The determination of the flows of the amines required a separate measurement of their viscosities. The viscosities were determined relative to the well-established values for H_2 and He. For Poiseuille flow through a fixed capillary from a fixed reservoir

$$[4] \quad \frac{\eta_1}{\eta_2} = \left(\frac{\Delta p}{\frac{1}{p}\frac{dp}{dt}}\right)_1 \left(\frac{\Delta p}{\frac{1}{p}\frac{dp}{dt}}\right)_2^{-1}$$

where η is the viscosity, Δp is the pressure drop across the capillary, and p is the pressure in the reservoir. The ratio of viscosities of two pure gases can, therefore, be determined directly from measurements of Δp, p, and the rate of fall of pressure, dp/dt, for the flow of the two gases through a fixed capillary. The viscosities measured for the amines at 296 ± 2 K were: 112 μP for CH_3NH_2, 92.9 μP for $C_2H_5NH_2$, 99.8 μP for $(CH_3)_2NH$, and 96 μP for $(CH_3)_3N$. Independent measurements with gases of known viscosities, *viz.* CO, N_2, and Ar, indicated an accuracy for this method of better than 5%.

All experiments were carried out at a room temperature of 296 ± 2 K.

Data Analysis

The analytical techniques used for the determination of rate and equilibrium constants from the raw flowing afterglow data for reactions of the type

$$[5] \quad A^- + BH \underset{k_r}{\overset{k_f}{\rightleftharpoons}} B^- + AH$$

have been described in detail previously (6). Expressions have been derived for obtaining, from a fit to the decay of the A^- signal, values for k_f when the extent of reverse reaction is negligible (the reaction is far removed from equilibrium) and for k_f and k_r when appreciable back reaction is taking place (the reaction approaches equilibrium). When equilibrium is actually attained the fitting procedure allows a determination only of unique values for the ratio of rate constants, *viz.* k_f/k_r. The expressions developed for these analyses take into account

the loss of A^- and B^- ions due to ambipolar radial and axial diffusion as well as effects introduced by the neutral gas inlet and sampling port. Equilibrium constants are obtained from the ion signal ratio, $(B^-)/(A^-)$, measured at equilibrium. Mass discrimination factors are deduced from the stoichiometry of reaction 5.

In previous equilibrium studies of reactions of type [5] the reactant gases BH and AH were of high ($\geqslant 99.9\%$) purity and the reactions proceeded generally in the absence of competing and secondary processes. This was often not the case for the systems investigated here. The commercially available amines contained impurities as large as 2% (liquid phase) and in several instances competing and secondary reactions were encountered. Consequently we had to consider in our analysis of some of the data the more general scheme represented by

$$\begin{array}{ccc} A^- + BH & \underset{k_r}{\overset{k_f}{\rightleftharpoons}} & B^- + AH \\ k_f' \downarrow BH(XH) & & k_r' \downarrow AH(YH) \\ k_f'' \downarrow AH(YH) & & k_r'' \downarrow BH(XH) \end{array}$$

where XH and YH are impurities present in BH and AH respectively and k' and k'' are the rate constants for competing or secondary reactions. The kinetic equations for this scheme were solved exactly (7); diffusion was neglected. Model calculations incorporating realistic values for the concentrations of the impurities and the various rate constants were performed to indicate the effect of competing as well as secondary reactions on the decay of the reactant ion, $d \ln [A^-]/dF_{BH}$, the rise of the product ion, $d \ln [B^-]/dF_{BH}$, the ratio plot, $d([B^-]/[A^-])/dF_{BH}$, and the mass discrimination plot, $d[A^-]/d[B^-]$, all at various flows of AH, F_{AH}. A number of special cases were considered. The following observations were made for values of $k_f = 1 \times 10^{-9}$ cm^3 molecule^{-1} s^{-1}, $k_r = 1 \times 10^{-11}$ cm^3 molecule^{-1} s^{-1} (*viz.* $K = 100$), $F_{BH} < 10^{19}$ molecule s^{-1}, 10^{17} molecule s^{-1} $< F_{AH} < 10^{20}$ molecule s^{-1}, and a reaction time of 10 ms. These reaction parameters and operating conditions are typical of the experiments whose results are reported in this paper.

(1) Further Reactions of A^- with AH(YH)

In studies of the equilibria for reactions of type [5], AH is added into the reaction region in large excess to that generated by reaction. The AH is usually added upstream of the ionizer since AH often serves as the source gas for A^-. Reactions of A^- with AH or an impurity YH in AH result in a depressed initial A^- signal and give rise to increased curvature in the A^- decay, a shallow maximum in the ratio plot and curvature in the mass discrimination plot whose initial slope will yield a low value for the mass discrimination factor. At sufficiently high values of F_{BH} the A^- signal approaches the unperturbed value and the ratio $[B^-]/[A^-]$ asymtotically approaches the unperturbed ratio. At moderate flows of BH the extent of deviation from the unperturbed behaviour will depend on the relative rates of the proton transfer reaction of A^- with BH and possible reactions of A^- with AH and YH.

For the systems under study and the adopted experimental operating parameters, $k_f[BH] \geqslant 100k_f''[AH]$ and $100k_f''[YH]$ at moderate flows of BH. Under these conditions the apparent values of k_f/k_r (determined from the fit to the A^- decay), K (determined from the ratio plot), and m (determined from the m plot) will be within 90% of the true values.

(2) Further Reactions of B^- with AH(YH)

Competing reactions of B^- with AH(YH) serve as sinks for B^- which may prevent the establishment of equilibrium even at large flows of BH. They lead to decreased curvature in the A^- decay, a maximum in the B^- signal prior to the establishment of an asymptotic value, an asymptotic approach to the unperturbed concentration ratio, $[B^-]/[A^-]$, and curvature in the mass discrimination plot whose initial slope will yield a high value for the mass discrimination factor. The extent of the deviation from the unperturbed behaviour will depend on the relative rates of the proton transfer reaction of B^- with AH and the competing reactions of B^- with AH and YH. For the systems under study and the adopted experimental operating parameters $k_r[AH] \geqslant k_r'[AH]$ and $k_r'[YH]$. Under these conditions the apparent value of k_f/k_r is within 10%, of K is within 1%, and of m is within 20% of the true value.

(3) Further Reactions of both A^- and B^- with AH(YH)

For the special case when $k_f'' = k_r'$ the reactions of B^- with AH(YH) and of A^- with

AH(YH) act to depress the product and reactant ion signals without altering the shapes of the various ion profiles, *viz.* d ln $[A^-]/dF_{BH}$, d ln $[B^-]/dF_{BH}$, $d([B^-]/[A^-])/dF_{BH}$, and $d[A^-]/d[B^-]$. Differences in these two rate constants of course lead to either case *1* or case *2*.

(4) Further Reactions of A^- with BH(XH)

For the operating conditions and reaction parameters typical of the studies reported here, the occurrence of reactions of A^- with BH and/or reactions of A^- with impurities, XH, does not lead to any characteristic perturbations in the shapes of the decay of A^-, the production of B^-, and the variation of $[B^-]/[A^-]$ with addition of BH(XH). The mass discrimination plot shows curvature at low $[A^-]$ and yields a value for m which is too high. The best fit to the A^- decay and the ratio plot would lead to values for an apparent equilibrium constant approximately equal to $(k_f + k_f')/k_r$ and/or $(k_f + k_f'[XH]/[BH])/k_r$. For the studies reported here $k_f' \leqslant 0.1\, k_f$ and $k_f[BH] \geqslant 0.02 k_f'[XH]$, so that the values of the apparent equilibrium constant should be within *ca.* 10% of the value of the true equilibrium constant.

(5) Further Reactions of B^- with BH(XH)

In contrast to competing reactions of A^- with BH(XH), secondary reactions of B^- with BH(XH) can have a marked influence on the shapes of the ion profiles characteristic of the unperturbed equilibrium. The curvature in the A^- decay will be decreased (if $k_r''[BH]$ or $k_r''[XH] > k_r[AH]$ the decay cannot be fitted with the standard analysis), the B^- production will reach a maximum at low additions of BH, the ratio $[B^-][AH]/[A^-][BH]$ will not converge to a constant value, and the sign of the slope of the mass discrimination plot will change at low $[A^-]$.

(6) Further Reactions of both A^- and B^- with BH(XH)

For the special case when $k_r'' = k_f'$ the ratio $[B^-][AH]/[A^-][BH]$ does converge to a constant value which provides a measure of the true equilibrium constant if the mass discrimination factor is known. The sign of the slope of the mass discrimination plot still changes at low $[A^-]$. The slope approaches the true value of m at high $[A^-]$, *viz.* in the limit of little conversion of A^- to B^-. The curvature in the A^- decay is still decreased and the B^- production still reaches a maximum value at low additions of BH. A fit to the curvature in the A^- decay will result in a high value for k_f/k_r.

Results

The extended analysis given above proved to be most valuable for predicting the operating conditions under which the rates of competing and/or secondary reactions were sufficiently depressed to allow an adequate determination of the true rate and equilibrium constants of the proton transfer reaction of interest with the application of the standard analysis. The shapes of the mass discrimination plots as well as, of course, the observed changes in the total mass spectrum proved to be the most sensitive indicators of the presence of competing and/or secondary reactions. In the experiments reported here special care was required to avoid complications which could be introduced by the occurrence of clustering reactions either of the type

$$A^- + AH + M \rightleftarrows A^- \cdot AH + M \quad [6a]$$

or of the type

$$B^- + BH + M \rightleftarrows B^- \cdot BH + M \quad [6b]$$

and by the occurrence of reactions with impurities in CH_3NH_2 and $C_2H_5NH_2$. This was accomplished either with a judicious choice of the flows of AH and BH and the reaction time or with a study of the reverse direction of reaction. Complications introduced by clustering reactions of the types

$$A^- + BH + M \rightleftarrows A^- \cdot BH + M \quad [6c]$$

$$B^- + AH + M \rightleftarrows B^- \cdot AH + M \quad [6d]$$

and two-body secondary or competing reactions with BH or AH were generally not encountered.

The rate and equilibrium constants determined for the reactions of types [2] and [3] investigated in this study are summarized in Tables 1 and 2. Only those values are included for whose determination the effects of competing and secondary reactions were negligible, so that the standard analysis was applicable. Under less ideal conditions the extended analysis was employed but only to establish further confidence in the results. The results obtained for the individual reactions are described in detail

TABLE 1. Summary of the experimentally determined values and precisions for $(k_f/k_r)_{ne}$, $(k_f/k_r)_e$ and K at 296 ± 2 K for proton transfer reactions of the type $X^- + YH \rightleftarrows Y^- + XH$ involving H_2, NH_3, and several amines

Reaction	$(k_f/k_r)_{ne}$[a]		$(k_f/k_r)_e$[a]				K[b]			
	N[c]	Forward	N[c]	Forward	N[c]	Reverse	N[c]	Forward	N[c]	Reverse
$NH_2^- + H_2 \rightleftarrows H^- + NH_3$	2	23±2 (8)	2	28±1 (8)			4	27±2 (8)		
$NH_2^- + CH_3NH_2 \rightleftarrows CH_3NH^- + NH_3$					3	2.44±0.18	5	2.25±0.13	3	2.44±0.20
$CH_3NH^- + H_2 \rightleftarrows H^- + CH_3NH_2$	4	13±2					3	11.0±0.2		
$NH_2^- + C_2H_5NH_2 \rightleftarrows C_2H_5NH^- + NH_3$	5	(1.3±0.3)×10³					4	(1.3±0.3)×10³		
$H^- + C_2H_5NH_2 \rightleftarrows C_2H_5NH^- + H_2$			1	65	1	76	1	80	3	83±27
$H^- + (CH_3)_2NH \rightleftarrows (CH_3)_2N^- + H_2$	2	(5.2±1.3)×10³	1	4.8×10³			2	(5.4±1.1)×10³		

[a]Analysis B (6).
[b]Analysis C (6).
[c]N represents the number of experimental determinations.

TABLE 2. Summary of the experimental measurements at 296 ± 2 K of rate constants (in units of 10^{-9} cm^3 molecule^{-1} s^{-1}) and equilibrium constants for proton transfer reactions of the type $X^- + YH \rightleftarrows Y^- + XH$ involving H_2, NH_3, and several amines

Reaction	$k_{forward}$[a]	N[b]	K[c]	N[b]
$NH_2^- + H_2 \rightleftarrows H^- + NH_3$	0.023±0.005 (8)	5	26±6 (8)	8
$NH_2^- + CH_3NH_2 \rightleftarrows CH_3NH^- + NH_3$	≥0.1		2.4±0.4	11
$CH_3NH^- + H_2 \rightleftarrows H^- + CH_3NH_2$	0.20±0.06	4	12±3	7
$NH_2^- + C_2H_5NH_2 \rightleftarrows C_2H_5NH^- + NH_3$	2.6±0.8	5	(1.3±0.4)×10^3	11
$H^- + C_2H_5NH_2 \rightleftarrows C_2H_5NH^- + H_2$	1.1±0.3	4	77±14	6
$H^- + (CH_3)_2NH \rightleftarrows (CH_3)_2N^- + H_2$	4.3±0.9	4	(5.2±1.1)×10^3	5
$NH_2^- + (CH_3)_2NH \rightleftarrows (CH_3)_2N^- + NH_3$	≃3			
$NH_2^- + (CH_3)_3N \rightarrow$	≲0.001			

[a] Values of $k_{forward}$ were determined using either Analysis A or B (6). The limits given along with the mean value represent the estimated accuracy.
[b] N is the number of experiments.
[c] The value for K represents the weighted mean together with its standard error of measurements including one or more of $(k_f/k_r)_c$, $(k_f/k_r)_{nc}$, and K_{ratio} in one or both directions of the reaction (6).

below. An account of the usual sources of error has been given previously (6).

In the remainder of this section the best estimate of a true value is taken to be the mean of a series of measurements. The limits given along with the mean value represent the best estimate of the precision (9).

[7] $NH_2^- + CH_3NH_2 \rightleftarrows CH_3NH^- + NH_3$

Figure 1 shows the variation of the dominant negative ions observed upon the addition of methylamine into a flowing NH_3–He plasma in which NH_2^- is initially a major negative ion. The behaviour shown is representative of the observations made in five separate experiments performed under similar conditions: effective reaction length, L = 60 cm, average flow velocity, $\bar{v}$ = 8.8–8.9 × 10^3 cm s^{-1}, total pressure, p = 0.426–0.452 torr, and flow of NH_3 = 1.19–1.27 × 10^{19} molecule s^{-1}. The ions CN^- and Cl^- which are usual impurity ions detected in the mass spectrum were also monitored but are not included in Fig. 1 as they were observed to be insensitive to the added CH_3NH_2. Helium was used as the buffer gas in all experiments and the NH_2^- ion was produced via electron impact of *ca.* 40 eV on NH_3.

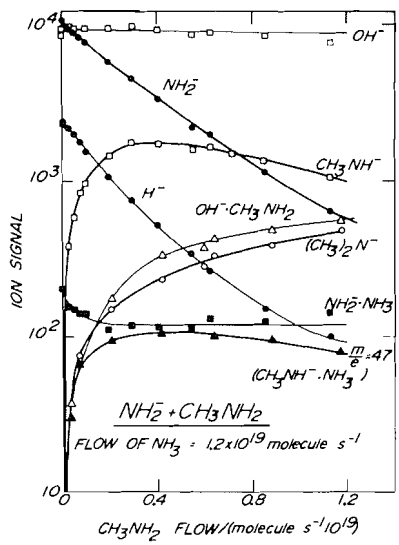

FIG. 1. The variation of the major negative ion signals recorded upon the addition of CH_3NH_2 into a flowing NH_3–He plasma in which NH_2^- is initially a major ion. T = 297 K, p = 0.433 torr, $\bar{v}$ = 8.8 × 10^3 cm s^{-1}, and L = 60 cm.

The decay of the NH_2^- signal and the accompanying increase in the CH_3NH^- signal can be attributed for the most part to the occurrence in the reaction region of the proton transfer reaction 7. For the adopted experimental conditions however, a number of alternate sinks and sources for NH_2^- and CH_3NH^- have to be considered.

Possible alternate sinks for NH_2^- are the displacement reaction

[7a] $NH_2^- + CH_3NH_2 \rightarrow H^- +$ Neutral products

and reactions with the major impurities, *viz.* H_2O, $(CH_3)_2NH$, and $(CH_3)_3N$, which are present in the CH_3NH_2 reactant gas

[8] $NH_2^- + H_2O \rightarrow OH^- + NH_3$

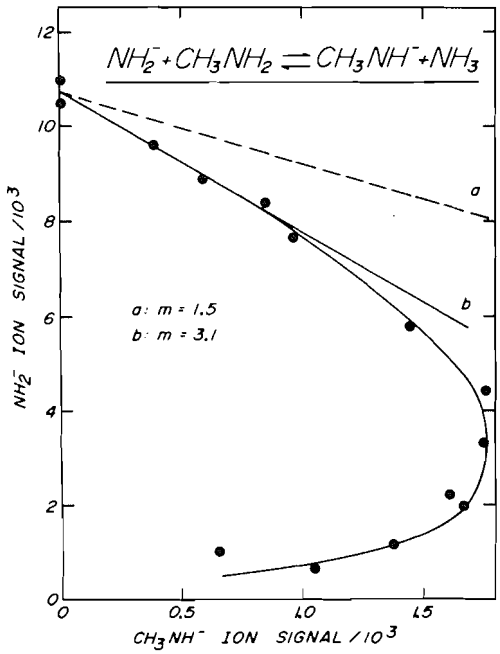

FIG. 2. A plot of the NH_2^- signal against the CH_3NH^- signal as a function of CH_3NH_2 addition for the data shown in Fig. 1. The curvature at low NH_2^- signals is indicative of secondary and/or competing reactions proceeding in either direction. Curve *a* is representative of the mass discrimination plot obtained from a study of the reverse direction of reaction which was observed to be uncomplicated by secondary or competing reactions. Curve *a* is normalized to the initial NH_2^- signal.

[9] $NH_2^- + (CH_3)_2NH \rightarrow (CH_3)_2N^- + NH_3$

Independent experiments which are discussed later in this section indicated that NH_2^- does not react rapidly with $(CH_3)_3N$. There was some evidence for the occurrence of reaction 7*a*; at very low flows of CH_3NH_2 the initial H^- signal actually increases slightly before decaying as a result of further reaction. The reactions with impurities are undoubtedly also occurring to some extent. The observed increase in the $(CH_3)_2N^-$ signal may result, at least in part, from the occurrence of reaction 9. The slight increase in the OH^- signal can be attributed to reaction 8. The ensuing decrease in the OH^- signal results from the three-body association reaction

[10] $OH^- + CH_3NH_2 + M \rightarrow OH^- \cdot CH_3NH_2 + M$

for which the product cluster is readily observed. An analysis of the observed increase in the $OH^- \cdot CH_3NH_2$ signal at low methylamine additions provided a value for $k_{10} \simeq 5 \times 10^{-29}$ cm^6 molecule^{-2} s^{-1}.

A number of reactions appear to be depleting the CH_3NH^- produced from reaction 7. Several secondary reactions with CH_3NH_2 are allowed on the basis of thermodynamic considerations

[11*a*] $CH_3NH^- + CH_3NH_2 \rightarrow NH_2^- + (CH_3)_2NH$

[11*b*] $\rightarrow (CH_3)_2N^- + NH_3$

[11*c*] $\rightarrow H^- +$ Neutral products

[11*d*] $\xrightarrow{M} CH_3NH^- \cdot CH_3NH_2$

One or more of these reactions may be responsible for the observed decrease in the CH_3NH^- signal at large methylamine additions. CH_3NH^- may also be depleted to some extent by proton transfer reactions with the H_2O and $(CH_3)_2NH$ impurities in CH_3NH_2. Finally, a fraction of the CH_3NH^- ions appear to be clustered with NH_3 (which is a fixed quantity in each experiment) as a result of the three-body association reaction

[12] $CH_3NH^- + NH_3 + M \rightarrow CH_3NH^- \cdot NH_3 + M$

An increase in the NH_3 flow was observed to result in an increase in the $CH_3NH^- \cdot NH_3$ production.

Reaction 11*a* represents a possible source of NH_2^- other than reaction '-7'. The proton transfer reaction

[-13] $H^- + CH_3NH_2 \rightarrow CH_3NH^- + H_2$

which accounts for the bulk of the H^- decay, represents an alternate source of CH_3NH^-. The H^- is also depleted to some extent as a result of fast proton transfer reactions with the H_2O and $(CH_3)_2NH$ impurities in methylamine.

The cluster ion $NH_2^- \cdot NH_3$, present in only small amounts in these experiments, appears not to react rapidly with CH_3NH_2. The initial decay in the $NH_2^- \cdot NH_3$ signal can be attributed entirely to the depletion in the reaction region of the precursor ion NH_2^-.

The observations shown in Fig. 1 and the considerations of the foregoing section indicate that the ion chemistry proceeding in the reaction region under the adopted experimental conditions is fairly complex. The mass discrimination plot shown in Fig. 2 provides further evidence of this complex behaviour. Such a plot should be linear with a slope of $-m$ if the proton transfer reaction 7 is the only reaction occurring,

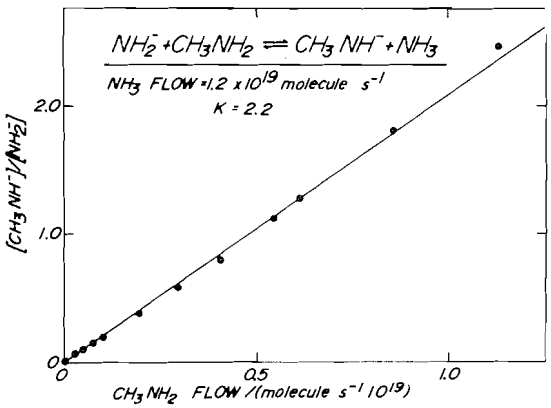

FIG. 3. The observed variation in the ratio of the product to the reactant ion signal corrected for mass discrimination, $[CH_3NH^-]/[NH_2^-]$, with addition of CH_3NH_2 at high back reactant NH_3 flows. T = 297 K, p = 0.433 torr, $\bar{v} = 8.8 \times 10^3$ cm s^{-1}, and L = 60 cm. The mass discrimination factor (m = 1.5) was determined from a study of the reaction in the reverse direction.

and will become non-linear in the presence of secondary and/or competing reactions. The shape of the m plot shown is consistent with the occurrence of competing reactions between NH_2^- and CH_3NH_2 (or impurity) and secondary reactions between CH_3NH^- and CH_3NH_2 (or impurity), cases *4* and *5* in the extended analysis, respectively. The curvature in the m plot of course prevents a direct determination of an accurate value for the mass discrimination factor (the initial slope provides only an upper limit). It was, therefore, decided to adopt the value of $m = 1.5 \pm 0.1$ determined from a study of reaction 7 in the reverse direction under similar sampling conditions. Included in Fig. 2 is a normalized mass discrimination plot obtained from a study of the reaction '−7' which was found to be uncomplicated by secondary and/or competing reactions.

Figure 3 shows the variation of the ratio of the product ion to reactant ion concentrations, $[CH_3NH^-]/[NH_2^-]$, as a function of the neutral reactant CH_3NH_2 flow for the data given in Fig. 1. This behaviour is representative of the observations made in all five experiments. Notwithstanding the complexity of the ion chemistry, the linearity of these ratio plots suggests that equilibrium is readily established, even for the lowest measurable additions of methylamine. The five measurements provided a value of $K = 2.25 \pm 0.13$ which should equal the value of the true equilibrium constant if the rates of secondary and/or competing reactions are not excessive. In order to obtain a measure of the extent of secondary and competing reactions the extended analysis was applied to a fit of the NH_2^- decay, the concomitant rise in the CH_3NH^- signal, and the mass discrimination plot. The extended analysis incorporated the reactions

[14] $NH_2^- + CH_3NH_2$ (impurity) → Products

[15] $CH_3NH^- + CH_3NH_2$ (impurity) → Products

Reactions 14 and 15 represent any or all of the possible competing and secondary reactions described above with methylamine and the impurities therein. The standard analysis which ignores reactions 14 and 15 allowed a fit to the NH_2^- decay only at low flows of CH_3NH_2. However, the extended analysis allowed a fit to the variation of both the NH_2^- and CH_3NH^- ions (and therefore the mass discrimination plot) over the entire range of CH_3NH_2 flows using the values $k_7/k_{-7} = 2.2$, $m = 1.4$, $k_7 = 15k_{14}$ and $k_{-7} = 10k_{15}$. Consequently, it appears that the rates of the competing and/or secondary reactions are not excessive and that the adopted value of m is in fact reasonable so that the value of K determined from the ratio plots should be very nearly equal to (within 10% of) the true value.

[−7] $CH_3NH^- + NH_3 \rightleftarrows NH_2^- + CH_3NH_2$

Reaction '−7' was investigated in order to minimize the complications due to competing and secondary reactions encountered in the study of reaction 7 and so to establish further confidence in the value for the equilibrium constant. The purity of the NH_3 is considerably better than that of CH_3NH_2 so that reactions with impurities present in the forward reactant will be reduced, while reactions with impurities in the methylamine, which is of constant concentration in the reaction region, will be unimportant so long as the rates of depletion of NH_2^- and CH_3NH^- are similar (case *3* in the extended analysis). This then leaves only complications due to any competing and secondary reactions with NH_3 and CH_3NH_2 as potential sources of error. Figure 4 shows the variation of the dominant negative ion signals recorded upon the addition of NH_3 into a CH_3NH_2–He plasma in which CH_3NH^- is initially a major negative ion. This behaviour is representative

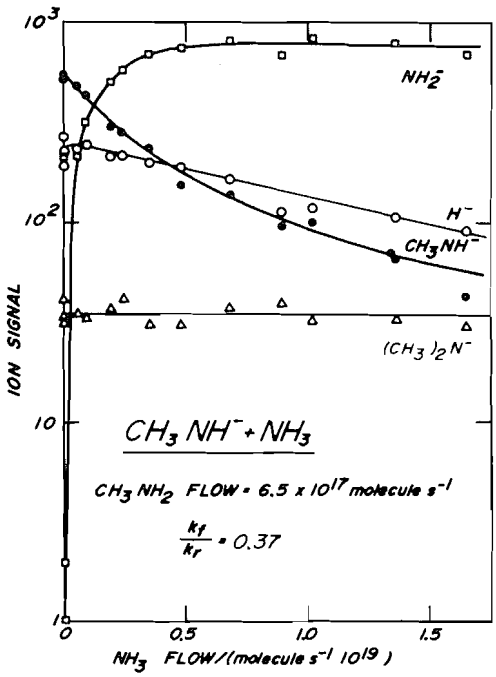

FIG. 4. The variation of the major negative ion signals recorded upon the addition of NH_3 into a flowing CH_3NH_2–He plasma in which CH_3NH^- is initially a dominant negative ion. The curve drawn through the observed CH_3NH^- decay represents a computed fit which yields a value for the ratio of rate constants, k_f/k_r, for the proton transfer reaction $CH_3NH^- + NH_3 \rightleftarrows NH_2^- + CH_3NH_2$. The ion observed at *m/e* 44 is presumed to arise from the $(CH_3)_2NH$ impurity in CH_3NH_2. $T = 298$ K, $p = 0.295$ torr, $\bar{v} = 9.3 \times 10^3$ cm s^{-1}, and $L = 59$ cm.

of the observations made in three separate experiments which were performed over the following range of reaction conditions: $L = 59$ cm, $p = 0.287$–0.296 torr, $\bar{v} = 9.3$–9.4×10^3 cm s^{-1}, and CH_3NH_2 flow $= 6.5 \times 10^{17} - 2.13 \times 10^{18}$ molecule s^{-1}. The usual impurity ions OH^-, CN^-, and Cl^- were also monitored but are not included in Fig. 4 as they were observed not to react rapidly with ammonia. The curvature in the decline of the reactant ion CH_3NH^- and the increase in the NH_2^- signal can be attributed to the occurrence of the proton transfer reaction '−7'. The observation that the $C_2H_6N^-$ ion (*m/e* 44) is insensitive to the addition of NH_3 is strongly suggestive that reaction 11*c*, while thermodynamically allowed, is nevertheless not a significant process at thermal energies. If this reaction were an important source of $(CH_3)_2N^-$ then the loss of its precursor ion CH_3NH^- would result in a corresponding decrease in the signal at *m/e* 44. Most likely the ion at *m/e* 44 observed in both the forward and reverse studies is $(CH_3)_2N^-$ arising from the dimethylamine impurity in the methylamine. Since NH_2^- and CH_3NH^- probably react with $(CH_3)_2NH$ with very similar rate constants the $(CH_3)_2N^-$ signal does not vary as reaction '−7' proceeds.

The H^- ion present in the CH_3NH_2–He plasma is in part a precursor of CH_3NH^- in the reaction region according to reaction '−13' which has a measured rate constant of $(1.6 \pm 0.5) \times 10^{-11}$ cm^3 $molecule^{-1}$ s^{-1}. Also, Bohme *et al.* (8) have established that H^- reacts with NH_3 according to

$$[-16] \qquad H^- + NH_3 \rightarrow NH_2^- + H_2$$

which has a measured rate constant of $(9.0 \pm 1.8) \times 10^{-13}$ cm^3 $molecule^{-1}$ s^{-1}. The decay of the H^- in Fig. 4 can therefore be attributed to reaction '−16' and, to a lesser extent, to the reaction of H^- with H_2O impurity in ammonia. Because of reaction '−13' the depletion of H^- by NH_3 contributes indirectly to the loss of CH_3NH^- in the reaction region. The decay of CH_3NH^- will of course also be influenced by any three-body contribution to the reaction of CH_3NH^- with NH_3, *viz.* 12. However, both these contributions to the CH_3NH^- decay were never sufficient to noticeably influence the ratio of rate constants obtained from the fit to the CH_3NH^- decay or the equilibrium constant obtained from the equilibrium ion and neutral concentrations present at the adopted experimental conditions. In all three experiments equilibrium was apparently attained for reaction '−7', already at the smallest additions of ammonia. This is demonstrated by the linearity at the lowest flows of NH_3 in the ratio plot shown in Fig. 5. Furthermore, the mass discrimination plots were observed to be linear over a large range of NH_3 flows. The slopes of these plots were independent of the CH_3NH_2 addition and provided an average value for $m = 0.67 \pm 0.04$. These results also provide a good indication that any further reactions of NH_2^- and CH_3NH^- with CH_3NH_2 (or impurity) and NH_3 (or impurity) do not sufficiently perturb the equilibrium under investigation to prevent the applicability of our standard equilibrium analysis. The three ratio plots yielded a mean value for K_{-7} of 0.41 ± 0.04. Fitting of the CH_3NH^- decay

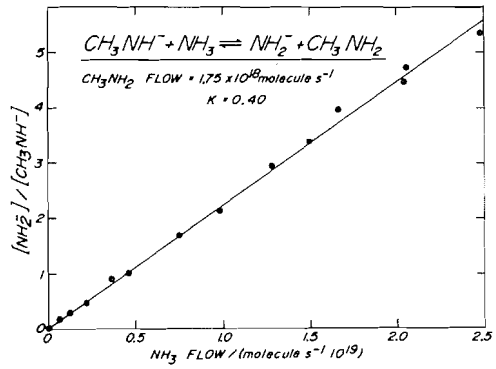

FIG. 5. The observed variation of the ion concentration ratio $[NH_2^-]/[CH_3NH^-]$, with NH_3 addition. The ion signal ratio was corrected for mass discrimination. The linearity of this plot indicates the attainment of equilibrium at all measured NH_3 flows. $T = 297$ K, $p = 0.287$ torr, $\bar{v} = 9.3 \times 10^3$ cm s^{-1}, $L = 59$ cm, and $m = 0.65$.

provided a unique value only for the ratio of rate constants $(k_{-7}/k_7)_e$. The mean value for $(k_{-7}/k_7)_e$ obtained from the three experiments was 0.41 ± 0.03. Fig. 4 includes a fit to the CH_3NH^- decay.

The initial slope in the decay of CH_3NH^- provides a lower limit for k_{-7} of $\sim 4 \times 10^{-11}$ cm^3 $molecule^{-1}$ s^{-1}. This result together with the observation that $k_{-7}/k_7 = 0.41$ provides a lower limit for k_7 of $\sim 1 \times 10^{-10}$ cm^3 $molecule^{-1}$ s^{-1}.

[13] $$CH_3NH^- + H_2 \rightarrow H^- + CH_3NH_2$$

The addition of H_2 to a CH_3NH_2–He plasma in which CH_3NH^- is initially a dominant ion resulted in the ion variation shown in Fig. 6. The entire decay of the CH_3NH^- signal was attributed to the proton-transfer reaction as there was no evidence for other reaction channels. Several alternative (thermodynamically allowed) reaction routes can be envisaged which result in the interconversion of CH_3NH^- and H^-, *viz.*

[17]

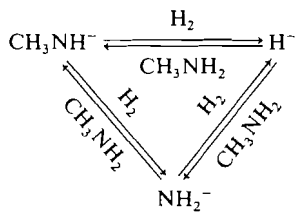

However there was no evidence for the rapid occurrence of these alternate routes; no NH_2^- was observed at low flows of H_2 and CH_3NH_2.

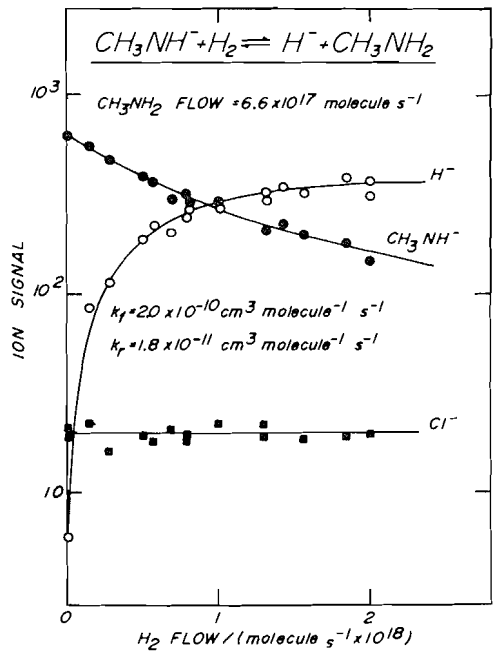

FIG. 6. A determination of the rate constants for the reaction of CH_3NH^- with H_2 from the best fit to the observed decay of CH_3NH^- upon addition of H_2 into a He–CH_3NH_2 plasma. $T = 297$ K, $p = 0.345$ torr, $\bar{v} = 8.3 \times 10^3$ cm s^{-1}, and $L = 60$ cm.

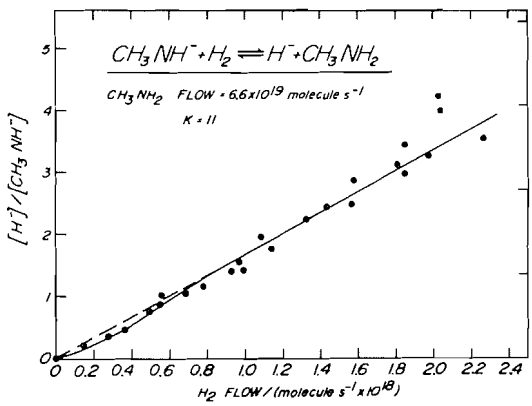

FIG. 7. The observed variation of $[H^-]/[CH_3NH^-]$ with H_2 flow showing the approach to and attainment of equilibrium for the reaction $CH_3NH^- + H_2 \rightleftarrows H^- + CH_3NH_2$. The best straight line through the data points at high H_2 flows yields a value for K of 11. $T = 297$ K, $p = 0.345$ torr, $\bar{v} = 8.3 \times 10^3$ cm s^{-1}, $L = 60$ cm, and $m = 1.4$.

Four separate experiments were performed over a range of flows of CH_3NH_2 from $3.84 \times 10^{17} - 6.6 \times 10^{18}$ molecule s^{-1}, a range of $\bar{v}$ from 8.3–9.1 $\times 10^3$ cm s^{-1}, and reaction lengths,

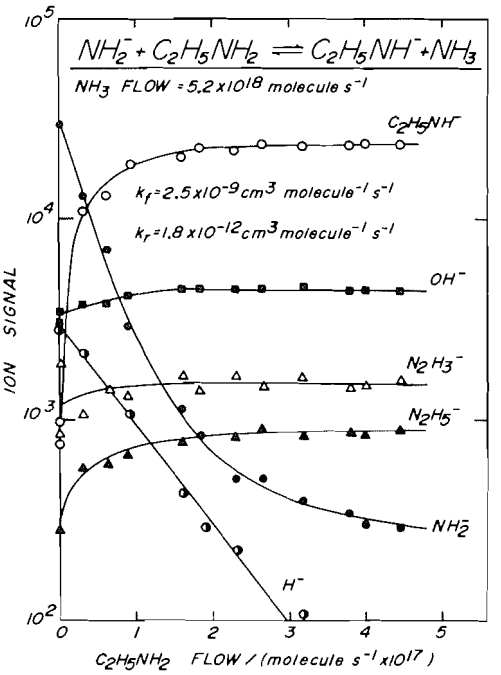

FIG. 8. The variation of the major negative ion signals recorded upon the addition of $C_2H_5NH_2$ into a NH_3–He plasma in which NH_2^- is initially dominant. The solid line drawn through the observed NH_2^- decay represents the best fit which provides the values indicated for the rate constants of the reaction $NH_2^- + C_2H_5NH_2 \rightleftarrows C_2H_5NH^- + NH_3$. $T = 295$ K, $p = 0.398$ torr, $\bar{v} = 8.2 \times 10^3$ cm s^{-1}, and $L = 85$ cm.

$L = 60$ and 84 cm. The total gas pressure, p, had values from 0.287–0.354 torr. Fitting of the four decays of CH_3NH^- using analysis B (6) resulted in unique values for both $k_{13} = (2.0 \pm 0.2) \times 10^{10}$ cm^3 molecule^{-1} s^{-1} and $k_{-13} = (1.6 \pm 0.3) \times 10^{-11}$ cm^3 molecule^{-1} s^{-1} and a mean value for $(k_{13}/k_{-13})_{nc} = 13 \pm 2$. In three of the four experiments equilibrium was established at high flows of H_2. Fig. 7 shows the ratio plot for one of these three experiments. The linear regions in all three ratio plots could be fitted with a value for $K_{13} = 11.0$.

[18] $NH_2^- + C_2H_5NH_2 \rightleftarrows C_2H_5NH^- + NH_3$

Figure 8 shows the variation of the dominant negative ion signals upon addition of $C_2H_5NH_2$ into a NH_3–He plasma in which NH_2^- is initially a major negative ion. Along with the usual unreactive impurity ions, ion signals were monitored at m/e 1, 16, 31, 33, and 44 which were identified as H^-, NH_2^-, $N_2H_3^-$, $N_2H_5^-$, and $C_2H_5NH^-$ respectively.

H^- initially present in the NH_3–He plasma reacts with $C_2H_5NH_2$ according to

[19] $H^- + C_2H_5NH_2 \rightarrow C_2H_5NH^- + H_2$

The $C_2H_5NH^-$ produced in this reaction contributes about 10% to the total $C_2H_5NH^-$ signal. The observed increases in the $N_2H_5^-$ and $N_2H_3^-$ signals can be ascribed either to additional channels for the forward reaction, *viz.*

[18*a*] $NH_2^- + C_2H_5NH_2 \rightarrow N_2H_5^- + C_2H_4$

[18*b*] $\rightarrow N_2H_3^- + C_2H_6$

or to additional channels for the reverse reaction, *viz.*

[−18*a*] $C_2H_5NH^- + NH_3 \rightarrow N_2H_5^- + C_2H_4$

[−18*b*] $\rightarrow N_2H_3^- + C_2H_6$

This latter possibility was however ruled out on the basis of the observed independence of the $C_2H_5NH^-/N_2H_5^-$ and $C_2H_5NH^-/N_2H_3^-$ ion signal ratios on the flow of NH_3. Finally the slight increase in the OH^- signal with $C_2H_5NH_2$ addition can be attributed to the reactions of H^-, NH_2^-, and $C_2H_5NH^-$ with H_2O impurity in $C_2H_5NH_2$ (10).

Five separate experiments were performed over a range of flows of NH_3 from 1.4–7.6 $\times 10^{18}$ molecule s^{-1} at total gas pressures, p, in the range 0.334–0.445 torr and effective reaction lengths, L, of 60 and 85 cm. The gas velocity, $\bar{v}$, had values in the range 8.1–8.6 $\times 10^3$ cm s^{-1}. The standard equilibrium analysis adequately reproduced the behaviour of the NH_2^- and $C_2H_5NH^-$ ion signals under these operating conditions. The mass discrimination factor, the ratio of rate constants, and the equilibrium constant were observed to be independent of the flow of NH_3 and $C_2H_5NH_2$. Apparently the rates of the competing and secondary reactions were low enough to leave the equilibrium undisturbed. The application of the standard fitting procedure to the five decays of NH_2^- yielded unique values for $k_{18} = (1.6 \pm 0.1) \times 10^{-9}$ cm^3 molecule^{-1} s^{-1}, $k_{-18} = (1.1 \pm 0.5) \times 10^{-12}$ cm^3 molecule^{-1} s^{-1} and $(k_{18}/k_{-18})_{nc} = (1.3 \pm 0.3) \times 10^3$. The fit to the decay of NH_2^- in one of these experiments is shown in Fig. 8. In four of these experiments and two additional experiments performed at higher flows of NH_3

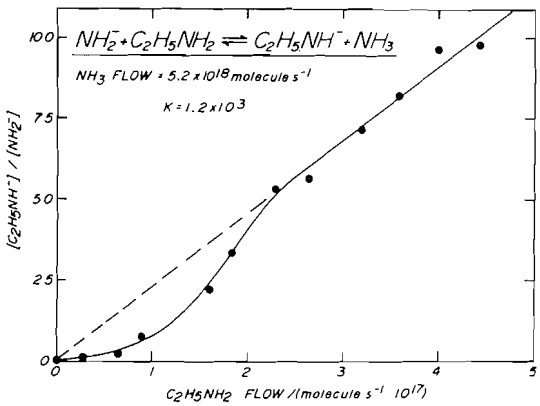

FIG. 9. The observed variation in the ion concentration ratio $[C_2H_5NH^-]/[NH_2^-]$ as a function of $C_2H_5NH_2$ addition showing the approach to and attainment of equilibrium for the reaction $NH_2^- + C_2H_5NH_2 \rightleftarrows C_2H_5NH^- + NH_3$. The best straight line through the points at high $C_2H_5NH_2$ flows yields a value of $K = 1.2 \times 10^3$. $T = 295$ K, $p = 0.398$ torr, $\bar{v} = 8.2 \times 10^3$ cm s^{-1}, $L = 85$ cm, and $m = 1.2$.

(1.9 and 4.4 $\times$ 10^{19} molecule s^{-1}) equilibrium was achieved at high flows of $C_2H_5NH_2$ as illustrated in Fig. 9. The slopes of the linear portions in the ratio plots yielded a value for $K_{18} = (1.3 \pm 0.3) \times 10^3$ which is in good agreement with the ratio of rate constants determined with the fitting procedure.

[19] $$H^- + C_2H_5NH_2 \rightleftarrows C_2H_5NH^- + H_2$$

The observed decay of the H^- signal and the accompanying rise in the $C_2H_5NH^-$ signal with addition of $C_2H_5NH_2$ into a NH_3–H_2–He plasma is shown in Fig. 10. The H^- is produced by electron impact on NH_3. Sufficient H_2, which acts as the back reactant in this experiment, was added downstream of the ionizer to remove NH_2^- prior to the reaction region via reaction 16 which also provides an additional source of H^-. The addition of small amounts of $C_2H_5NH_2$ into the reaction region gave rise to sampling effects reminiscent of our experiences with NH_3 (8) and also CH_3NH_2. The sampling effects which are evidenced by the sharp initial increase in the Cl^- signal shown in Fig. 10 discouraged an extensive study of this reaction in this direction. At higher additions of $C_2H_5NH_2$ the ion signals stabilize to reproducible values. The fit to the H^- decay shown in Fig. 10 gave a value for $(k_{19}/k_{-19})_c = (7 \pm 3) \times 10$ whereas the ratio plot shown in Fig. 11 yielded $K_{19} =$

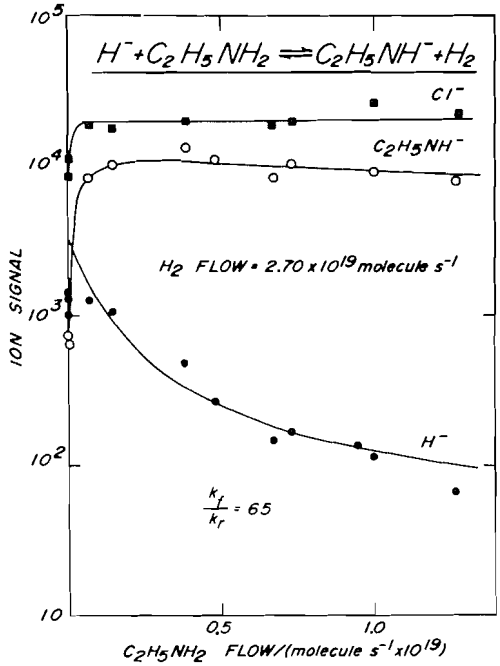

FIG. 10. The variation of major negative ion signals recorded upon the addition of $C_2H_5NH_2$ into a NH_3–H_2–He plasma. The solid line drawn through the observed H^- decay represents the fit which provides the value indicated for k_f/k_r of the reaction $H^- + C_2H_5NH_2 \rightleftarrows C_2H_5NH^- + H_2$. $T = 298$ K, $p = 0.316$ torr, $\bar{v} = 8.4 \times 10^3$ cm s^{-1}, and $L = 59$ cm. The flow of $NH_3 = 5 \times 10^{17}$ molecule s^{-1}.

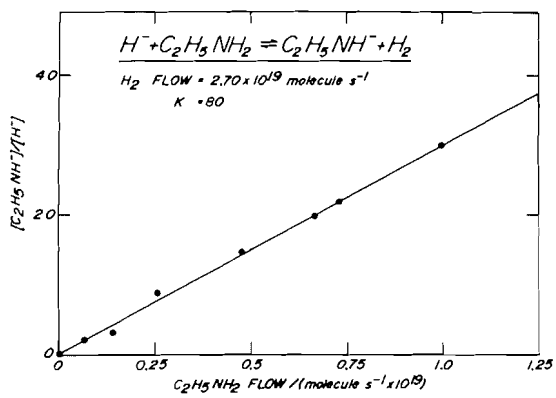

FIG. 11. The observed variation in $[C_2H_5NH^-]/[H^-]$ as a function of $C_2H_5NH_2$ flow for the data shown in Fig. 10. The best straight line through the points yields a value for $K = 80$. $m = 0.4$.

$(8 \pm 3) \times 10$. The large uncertainty in the value for K arises from the uncertainty introduced in the determination of the mass dis-

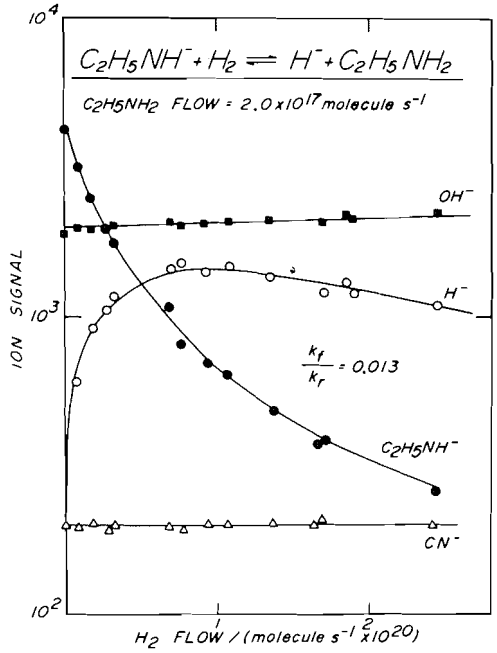

FIG. 12. The variation of the reactant $C_2H_5NH^-$ and product H^- ions upon the addition of H_2 into a $C_2H_5NH_2$–He plasma in which $C_2H_5NH^-$ is initially a dominant ion. The solid line through the $C_2H_5NH^-$ decay is a fit which provides a value for k_f/k_r of 0.013. T = 298 K, p = 0.309 torr, $\bar{v}$ = 8.9 × 10^3 cm s^{-1}, and L = 59 cm.

crimination factor by the unfavourable sampling conditions.

The rate constant for reaction 19 was determined from the earlier studies of reaction 18. In these latter experiments the small amounts of H^- present in the absence of H_2 were observed to react rapidly with $C_2H_5NH_2$ (see Fig. 8) with a rate constant k_{19} = (1.1 ± 0.1) × 10^{-9} cm^3 molecule^{-1} s^{-1}.

$$[-19] \quad C_2H_5NH^- + H_2 \underset{k_f}{\overset{k_r}{\rightleftharpoons}} H^- + C_2H_5NH_2$$

The decay of the $C_2H_5NH^-$ signal and the concomitant increase in the product H^- signal observed upon the addition of hydrogen into a $C_2H_5NH_2$–He plasma is shown in Fig. 12. The slight increase in the OH^- signal with H_2 addition may be attributed to the proton transfer reactions of H^- and $C_2H_5NH^-$ with H_2O both of which are rapid at 297 K (10). The water vapour impurity arises from two sources, that present in the back reactant $C_2H_5NH_2$, and that introduced with the H_2. The rate constant for the reaction of H^- with H_2O is almost three times as large as the rate constant for the reaction of $C_2H_5NH^-$ with H_2O so that part of the increase in the OH^- signal will arise from the more rapid reaction of the product H^- with the water vapour present in the back reactant ethylamine. The slight decrease in the H^- signal at large hydrogen flows may be ascribed to the reaction of H^- with the H_2O present in the forward reactant hydrogen. Three experiments were carried out under the following range of conditions: $\bar{v}$ = 8.4–8.9 cm^3 s^{-1}, p = 0.309–0.316 torr, L = 59 and 85 cm, and $C_2H_5NH_2$ flow = 1.75–7.3 × 10^{17} molecule s^{-1}. The maximum H_2 flow was 2.4 × 10^{20} molecule s^{-1}. An extended analysis which included the further reaction of both H^- and $C_2H_5NH^-$ with the quoted levels of water impurity in the H_2 and $C_2H_5NH_2$ indicated that the standard analysis of the $C_2H_5NH^-$ decay under these operating conditions should provide values for the rate constants within 10% of the true values for flows of $C_2H_5NH_2$ below ~3 × 10^{17} molecule s^{-1}. Figure 12 shows a fit to the $C_2H_5NH^-$ decay as determined with the standard analysis. This fit provided a value for k_{-19}/k_{19} = 0.013. The extended analysis also indicated that the occurrence of the reactions of H^- and $C_2H_5NH^-$ with the H_2O impurities in H_2 and $C_2H_5NH_2$ would not noticeably influence the determination of the equilibrium constant from the equilibrium concentrations present under the chosen operating conditions and that the true value of the mass discrimination factor could be obtained from the data taken at low flows of hydrogen. The ratio plot of the data shown in Fig. 12 is displayed in Fig. 13. It provided a value for K_{-19} = 0.010. In all three experiments equilibrium was established already at the lowest flows of H_2 used. The three ratio plots provided a mean value for K = 0.012 ± 0.004.

$$[20] \quad H^- + (CH_3)_2NH \rightleftarrows (CH_3)_2N^- + H_2$$

Figure 14 shows the variation in the major negative ion signals upon the addition of dimethylamine into a NH_3–H_2–He plasma in which H^- is initially a major negative ion. Of the ions monitored in the range m/e 1–50, only the ions with m/e 1 (H^-) and m/e 44 ($(CH_3)_2N^-$) responded significantly to the addition of dimethylamine. Figure 14 also includes the behaviour of the m/e 46 (NO_2^-) signal which

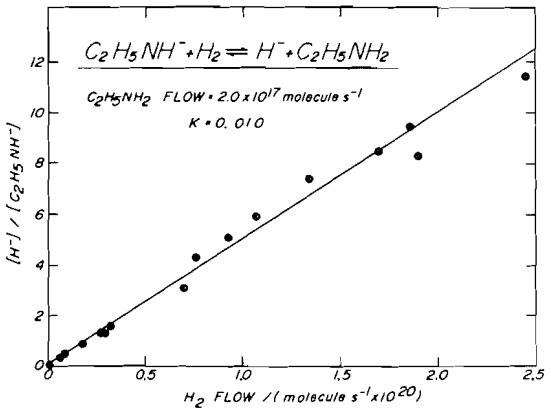

FIG. 13. The variation of the ratio of the product to reactant ion concentrations, $[H^-]/[C_2H_5NH]$, with H_2 addition for the data shown in Fig. 12. m = 2.4.

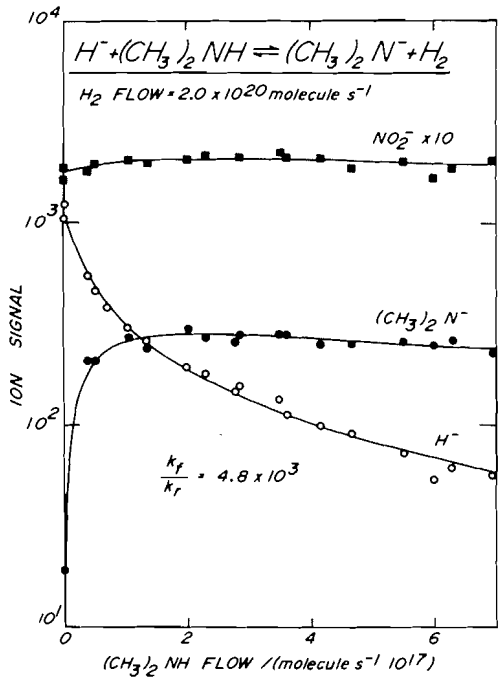

FIG. 14. The determination of the ratio of rate constants for the reaction $H^- + (CH_3)_2NH \rightleftarrows (CH_3)_2N^- + H_2$ from the best fit to the observed decay of H^- upon the addition of $(CH_3)_2NH$ into a NH_3–H_2–He plasma at high fixed H_2 flow. T = 296 K, p = 0.457 torr, $\bar{v}$ = 8.7 × 10^3 cm s^{-1}, and L = 85 cm. The flow of NH_3 = 3.5 × 10^{19} molecule s^{-1}.

typifies the usual behaviour of an unreactive impurity ion.

Three separate experiments were performed over a range of hydrogen flows (1.10 × 10^{18}–

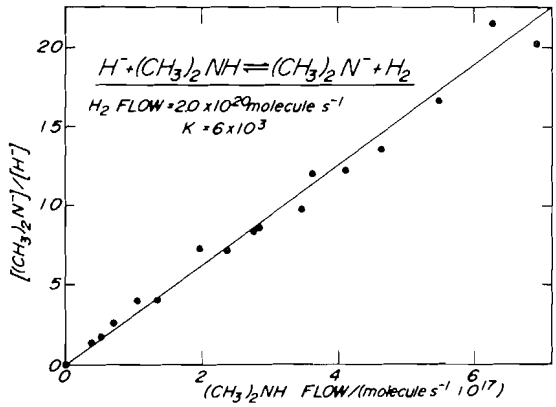

FIG. 15. The variation of the ratio of the product to reactant ion concentrations, $[(CH_3)_2N^-]/[H^-]$, with $(CH_3)_2NH$ addition for the data shown in Fig. 14. m = 3.8.

1.98 × 10^{20} molecule s^{-1}) and $(CH_3)_2NH$ flows (0–7.0 × 10^{17} molecule s^{-1}) sufficiently large to allow the determination of unique values for k_{20} and k_{-20} from a fit to the H^- decay and K_{20} from equilibrium concentrations using the standard analysis. The pressure had values in the range 0.372–0.457 torr, $\bar{v}$ had values in the range 8.2–8.7 × 10^3 cm s^{-1} and L had values of 60 and 85 cm. In two experiments the hydrogen flow was sufficiently low to permit the determination of unique values for k_{20} = (4.30 ± 0.4) × 10^{-9} cm^3 $molecule^{-1}$ s^{-1} and k_{-20} = (8.7 ± 1.2) × 10^{-13} cm^3 $molecule^{-1}$ s^{-1} from fits to the H^- decay. The third experiment, the data for which is shown in Fig. 14, provided only a unique value for the ratio of rate constants k_{20}/k_{-20} = 4.8 × 10^3. One additional experiment was carried out in which hydrogen back reactant was not added. A fit to the exponential decay of the H^- signal provided a value for the forward rate constant k_{20} = 4.2 × 10^{-9} cm^3 $molecule^{-1}$ s^{-1}. In two of the experiments equilibrium was established. One of the ratio plots is shown in Fig. 15. The linear portions of the two ratio plots provided a mean value for K_{20} of (5.4 ± 1.1) × 10^3. Due to the large value of the equilibrium constant no attempt was made to investigate reaction 20 in the reverse direction.

[21] $NH_2^- + (CH_3)_2NH \rightleftarrows (CH_3)_2N^- + NH_3$

One experiment was performed to investigate the proton transfer reaction 21 in a flowing NH_3–He plasma. Due to the large value of the

TABLE 3. Changes in the standard free energy, standard entropy, and standard enthalpy at 298 K for proton transfer reactions of the type $X^- + YH \rightleftarrows XH + Y^-$ involving H_2, NH_3, and several amines

Reaction	$-\Delta G^0_{298}$/(kcal mol^{-1})	ΔS^0_{298}/(eu)	$-\Delta H^0_{298}$/(kcal mol^{-1})
$NH_2^- + H_2 \rightleftarrows H^- + NH_3$	1.9±0.2 (8)	−4.3±0.5 (8)	3.2±0.4 (8)
$NH_2^- + CH_3NH_2 \rightleftarrows CH_3NH^- + NH_3$	0.51±0.10	+0.4±1.6	0.4±0.6
$CH_3NH^- + H_2 \rightleftarrows H^- + CH_3NH_2$	1.5±0.2	−4.5±1.0	2.8±0.5
$NH_2^- + C_2H_5NH_2 \rightleftarrows C_2H_5NH^- + NH_3$	4.2±0.2	+0.8±1.6	4.0±0.7
$H^- + C_2H_5NH_2 \rightleftarrows C_2H_5NH^- + H_2$	2.6±0.2	+5.1±1.0	1.1±0.5
$H^- + (CH_3)_2NH \rightleftarrows (CH_3)_2N^- + H_2$	5.0±0.1	+3.5±1.0	4.0±0.4

equilibrium constant, $\sim 10^5$, and unstable sampling conditions at the required flows of ammonia and dimethylamine, reaction 21 was not studied under equilibrium conditions. From the decay of the NH_2^- ion at moderate $(CH_3)_2NH$ flows it was possible from this one experiment to determine a value for $k_{20} \sim 3 \times 10^{-9}$ cm^3 molecule^{-1} s^{-1}. The conditions under which this experiment was carried out were: $p = 0.367$ torr, $\bar{v} = 8.6 \times 10^3$ cm s^{-1}, $L = 60$ cm, and NH_3 flow $= 2.9 \times 10^{17}$ molecule s^{-1}.

[22] $NH_2^- + (CH_3)_3N \rightleftarrows (CH_3)_2NCH_2^- + NH_3$

An investigation of reaction 22 was carried out again in a NH_3–He plasma in order to assess whether any of the methyl protons were acidic enough to be abstracted by NH_2^-. For large additions of trimethylamine ($\sim 1 \times 10^{19}$ molecule s^{-1}) the NH_2^- ion was observed to decline slowly with an accompanying increase in the ion signals at *m/e* 31, 34, and 44 which were identified as CH_3NH^-, $OH^- \cdot NH_3$, and $(CH_3)_2N^-$ respectively. A careful search was made for the ion $(CH_3)_2NCH_2^-$ (*m/e* 58), which would be the product of reaction 22, for the conditions: $p = 0.336$ torr, $\bar{v} = 8.1 \times 10^3$ cm s^{-1}, $L = 59$ cm, NH_3 flow $= 1.7 \times 10^{18}$ molecule s^{-1}, and $(CH_3)_3N$ flows up to 1×10^{19} molecule s^{-1}. The failure to observe $(CH_3)_2NCH_2^-$ over this range of flows suggests an upper limit to the rate constant for reaction 22 of 1×10^{-12} cm^3 molecule^{-1} s^{-1}. The majority of the observed decay of the NH_2^- signal could therefore be attributed to proton transfer reactions with the impurities H_2O, CH_3NH_2, and $(CH_3)_2NH$ present in the $(CH_3)_3N$. All of these reactions are rapid, and the rate constant for the depletion of NH_2^- determined from the slope of the NH_2^- decay, $k = 3.8 \times 10^{-11}$ cm^3 molecule^{-1} s^{-1}, was consistent with the total rate constant expected from the quoted impurity level of $\sim 1\%$. However, a part of the increase in the *m/e* 44 signal could have been due to the displacement reaction

[22*a*] $NH_2^- + (CH_3)_3N \rightarrow (CH_3)_2N^- + CH_3NH_2$

and/or the reaction

[22*b*] $NH_2^- + (CH_3)_3N \rightarrow C_2H_5NH^- + CH_3NH_2$

Discussion

Table 1 indicates the agreement between the measured ratios of rate constants determined from fits to the primary ion decays (and independent of mass discrimination) and the measured equilibrium ion concentrations (corrected for mass discrimination) together with their observed independence on the direction of approach to equilibrium. These results, together with the observed constancy of the measured ratios of rate constants and equilibrium constants over the range of reaction times and neutral concentrations adopted in these experiments, provide confidence that these measured values represent true equilibrium constants (6, 11). Further confidence is provided by the internal consistency between single-step and multi-step measurements. The equilibrium constant of 26 ± 6 determined directly from a study of the NH_3/H_2 system (8) compares favourably with the equilibrium constants of 29 ± 12 and 17 ± 8 determined indirectly from a study of the NH_3/CH_3NH_2 and CH_3NH_2/H_2 systems and the $NH_3/C_2H_5NH_2$ and $C_2H_5NH_2/H_2$ systems, respectively. The measured equilibrium constants summarized in Table 2 should therefore provide values for changes in the standard Gibbs free energy, ΔG^0_{298}, according to the relation

[23] $$\Delta G^0_T = -RT \ln K_T$$

TABLE 4. Absolute intrinsic acidities of amines at 298 K

$RH \rightleftarrows R^- + H^+$	ΔG^0_{298}/(kcal mol^{-1})
$H_2 \rightleftarrows H^- + H^+$	394.2±0.5 (12)
$NH_3 \rightleftarrows NH_2^- + H^+$	396.1±0.7 (8)
$CH_3NH_2 \rightleftarrows CH_3NH^- + H^+$	395.7±0.7
$C_2H_5NH_2 \rightleftarrows C_2H_5NH^- + H^+$	391.7±0.7
$(CH_3)_2NH \rightleftarrows (CH_3)_2N^- + H^+$	389.2±0.6
$(CH_3)_3N \rightleftarrows (CH_3)_2NCH_2^- + H^+$	>396

The thermodynamics of the proton transfer reactions may be specified further by estimating the standard entropy changes, ΔS^0_{298}, from the known or estimated entropies of the individual species (12) and then calculating the standard enthalpy changes, ΔH^0_{298}, according to the relation

$$[24] \qquad \Delta H^0_T = \Delta G^0_T + T\Delta S^0_T$$

The results of these calculations are summarized in Table 3. The entropies of the amide ions CH_3NH^-, $C_2H_5NH^-$, and $(CH_3)_2N^-$ were assumed to be equal to the entropies (13) of the isoelectronic species CH_3OH, C_2H_5OH, and $(CH_3)_2O$ respectively.

ΔG^0_{298} for reactions of types [2] and [3] is a measure of the difference in the intrinsic acidity of the pairs of Brønsted acids H_2 and R_1R_2NH and NH_3 and R_1R_2NH, respectively. Absolute values for the intrinsic acidities of the amines, R_1R_2NH, can therefore be derived from the values of ΔG^0_{298} in Table 3 when reference is made to the well-established intrinsic acidity of H_2. The relative acidity of H_2 and NH_3 has been measured previously (8). The resulting acidities are summarized in Table 4 and the scale of acidities shown in Fig. 16. The order of acidity, *viz.* dimethylamine > ethylamine > methylamine > ammonia is consistent with that first determined by Brauman and Blair (2) with their ion cyclotron resonance and pulsed double-resonance spectroscopy techniques. However, the absolute magnitudes of the differences in acidity show an unexpected pattern. The acidity increase from NH_3 to CH_3NH_2 is only 0.4 kcal mol^{-1} while the corresponding increase from CH_3NH_2 to $(CH_3)_2NH$ is 6.5 kcal mol^{-1}. Furthermore there is a rather large increase of 4.0 kcal mol^{-1} from CH_3NH_2 to $C_2H_5NH_2$.

The observed order of increasing acidity of the amines with increasing alkyl substitution

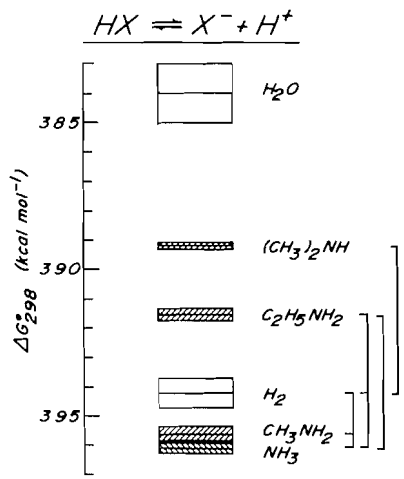

FIG. 16. Scale of intrinsic acidities. The measured relative acidities of pairs of Brønsted acids are represented by the brackets shown on the right hand side. The scale is set by the well established value of the acidity of H_2. The shaded rectangles indicate the experimental uncertainty in acidity relative to the acidity of H_2. The uncertainty in the absolute acidity is indicated for H_2 and H_2O which is included for comparison.

has been rationalized by Brauman and Blair (2) in terms of a model in which the charge localized on the N atom of the conjugate base is stabilized by the alkyl group acting as a polarizable medium. Such a model has also been invoked to explain the acidity orders observed for aliphatic alcohols (14) and monosubstituted carboxylic acids (15), acetylenes (16), and phenols (17). However, a 'first member anomaly' is observed in the latter groups of acids (except *o*-substituted phenols) in the sense that formic acid, acetylene, and phenol have acidities which are unexpectedly large relative to the acidities of the other members of their homologous series. For the acidities of the amines reported in this study the small difference in acidity between NH_3 and CH_3NH_2 compared to the larger differences between CH_3NH_2 and $(CH_3)_2NH$ as well as between CH_3NH_2 and $C_2H_5NH_2$ may also reflect a similar anomaly in that the acidity of NH_3 can be regarded to be unexpectedly large. The first member anomaly has been explained qualitatively in the case of the acetylenes and carboxylic acids in terms of a superimposition in the conjugate base of intrinsic permanent dipole and intramolecular induced dipole effects which act to localize and delocalize respectively the charge on the site in the

TABLE 5. A comparison of experimental and calculated proton affinities (in kcal mol^{-1}) of anions

R^-	Measured[a]	Calculated[b]		
		Hopkinson *et al.* (5)	Radom (4)	Hehre and Pople (3)
H^-	400.4±0.5 (12)	400.5[c]		
NH_2^-	403.6±0.9 (8)	421.9[c]		553.3
CH_3NH^-	403.2±1.0		442.8, 537.5	539.0
$C_2H_5NH^-$	399.4±1.0		439.3, 536.2	
$(CH_3)_2N^-$	396.4±0.9			523.8

[a]PA = ΔH^0_{298} for the reaction $RH \rightleftarrows R^- + H^+$.
[b]PA = ΔE.
[c]ΔE corrected for zero point vibration.

TABLE 6. Standard heats of formation of amide ions, the electron affinities of the corresponding radicals, and pertinent thermochemical information in kcal mol^{-1}. Values determined in this study are underlined

RH	$\Delta H^0_{f,298}(RH)$	$\Delta H^0_{f,298}(R)$	$\Delta H^0_{f,298}(R^-)$	EA(R)
H_2	0	52.100±0.001 (12)	33.2±0.5 (12)	18.9±0.5 (12)
NH_3	−10.97±0.1 (12)	44.3±1.1 (8)	25.4±1.0 (8)	18.9±0.1 (8)
CH_3NH—H	−5.5±0.5 (13)	43.6±2.0 (18)	<u>30.5±1.5</u>	<u>13.1±3.5</u>
C_2H_5NH—H	−11.0±0.5 (13)	38±2[a]	<u>21.2±1.5</u>	<u>17±4</u>
$(CH_3)_2N$—H	−4.5±0.5 (13)	39±2 (18)	<u>24.7±1.4</u>	<u>14.3±3.4</u>

[a]Calculated from $D^0_{298}(C_2H_5NH—H) \simeq D^0_{298}(CH_3NH—H) = 101 \pm 2$ kcal mol^{-1} (2).

anion from which the proton was removed. It is questionable whether a similar explanation is also appropriate in the case of the amines. Further measurements of acidities of other homologous series should provide a more complete and quantitative appreciation of all the factors which influence gas-phase acidity. The only quantitative assessment which is possible at this time is provided by quantum mechanical calculations of proton removal energies.

A number of quantum mechanical calculations of proton removal energies have recently been attempted for amines. Table 5 includes the results of *ab initio* molecular orbital studies reported by Hopkinson *et al.* (5), Radom (4), and Hehre and Pople (3). Although the calculations differ appreciably in quality according to the choice of the basis sets, they all correctly reproduce the observed order of proton affinity of the amide ions in the gas phase. However, the calculated absolute energies for proton removal are consistently higher than the experimental values by as much as ~35%. Better agreement (within ~10%) is obtained with the more extensive basis sets. Differences in intrinsic acidities also appear to be reproduced more accurately with the extensive sets. For example, the measured proton affinity difference of 3.8 ± 2.0 kcal mol^{-1} for $PA(CH_3NH^-)$–$PA(C_2H_5NH^-)$ compares more favourably (in fact remarkably well) with the value of 3.5 kcal mol^{-1} obtained by Radom (4) with the extended 4-31G set than the value of 1.3 kcal mol^{-1} obtained with the minimal STO-3G set.

The experimentally determined values of ΔH^0_{298} given in Table 3 for reactions of types [2] and [3] provide a measure of $\Delta H^0_{f,298}(R_1R_2N^-)$, $EA(R_1R_2N)$, and $PA(R_1R_2N^-)$ according to the relations

$$[25]\quad \Delta H^0_f(R_1R_2N^-) = \Delta H^0_f(R_1R_2NH) - \Delta H^0_f(RH) + \Delta H^0_f(R^-) - \Delta H^0$$

$$[26]\quad EA(R_1R_2N) = \Delta H^0_f(R_1R_2N) - \Delta H^0_f(R_1R_2N^-)$$

$$[27]\quad PA(R_1R_2N^-) = \Delta H^0 + PA(R^-)$$

where R = H or NH_2. The heats of formation of the amide ions and the electron affinities obtained in this manner are given in Table 6 and the proton affinities of the amide ions are summarized in Table 5. The trend in electron affinity with alkyl substitution of the amino radical also supports the notion that polarizable alkyl groups disperse negative charge from a

TABLE 7. Rate constants (in units of 10^{-9} cm^3 molecule^{-1} s^{-1}) and apparent activation energies for exothermic proton-transfer reactions involving H_2, NH_3, and several amines in the gas phase at 296 ± 2 K

Reaction	k_{expt}	$k_{capture}$[a]	$k_{expt}/k_{capture}$	E_a[b] (kcal mol^{-1})	$-\Delta H^0_{298}$ (kcal mol^{-1})
$NH_2^- + H_2 \rightarrow H^- + NH_3$	0.023±0.005	1.56[c]	0.015±0.003	2.5±0.1	3.2±0.3
$CH_3NH^- + H_2 \rightarrow H^- + CH_3NH_2$	0.20±0.06	1.52[c]	0.13±0.04	1.2±0.2	2.8±0.4
$NH_2^- + CH_3NH_2 \rightarrow CH_3NH^- + NH_3$	≥0.1	2.04[d]	≥0.05	≤2	0.41±0.45
$H^- + C_2H_5NH_2 \rightarrow C_2H_5NH^- + H_2$	1.1±0.3	7.62[e]	0.14±0.04	1.2±0.2	1.1±0.4
$NH_2^- + C_2H_5NH_2 \rightarrow C_2H_5NH^- + NH_3$	2.6±0.8	2.20[e]	1.2±0.4	0	3.9±0.5
$H^- + (CH_3)_2NH \rightarrow (CH_3)_2N^- + H_2$	4.3±0.8	7.04[f]	0.61±0.14	0.3±0.2	4.0±0.3
$NH_2^- + (CH_3)_2NH \rightarrow (CH_3)_2N^- + NH_3$	~3	1.90[f]	~1.5	0	7.2±0.6

[a] Calculated according to equation 28 in the text.
[b] The uncertainty in E_a reflects only the uncertainty in k_{expt}.
[c] α = 0.79 Å^3 (22).
[d] α = 3.92 Å^3 (22), μ_D = 1.27 D (23), c = 0.169 (21).
[e] α = 5.86 Å^3 (estimated from bond polarizabilities ref. 24), μ_D = 1.22 D (23), c = 0.165 (21).
[f] α = 5.59 Å^3 (estimated from bond polarizabilities, ref. 24), μ_D = 1.03 D (23), c = 0.150 (21).

charged centre and that larger alkyl groups do so more effectively (2, 4).

Recent room temperature measurements of the rate constants for a large number of exothermic proton-transfer reactions between simple inorganic and organic species proceeding in the gas phase have indicated that the transfer of a proton usually proceeds on nearly every collision, *viz.* that the reaction rate constant usually is very nearly equal to the capture rate constant (19). For reactants having a M.B. energy distribution, current classical theories of ion–molecule interaction predict a capture rate constant given by

$$[28] \quad k_c = 2\pi e \left(\frac{\alpha}{\mu}\right)^{1/2} + C\left(\frac{2\pi e \mu_D}{\mu}\right)\left(\frac{2\mu}{\pi k T}\right)^{1/2}$$

where e is the charge on the ion, μ the reduced mass of the collidants, α is the polarizability and μ_D is the permanent dipole moment of the neutral molecule (20, 21). C is a measure of the extent to which the dipole is oriented with respect to the direction of the approaching ion and can be determined from the ratio $\mu_D/\alpha^{1/2}$ (21). Table 7 presents a comparison of the rate constants measured for the proton transfer reactions investigated in this study with calculated capture rate constants. Although several of these reactions also proceed at essentially the capture rate, the specific rates of the reactions of NH_2^- and CH_3NH^- with H_2 and H^- with $C_2H_5NH_2$ deviate significantly from the predicted capture rate constants. The reasons for these deviations are not understood. Details of the potential energy surfaces for the relevant reaction intermediates (the classical theories of collision completely ignores short-range interactions) are not available. Should the low reaction efficiency be a consequence of the presence of a barrier in the potential energy surface, one can attempt to estimate the magnitude of such a barrier in the traditional Arrhenius manner (25) according to the equation

$$[29] \quad k_{exptl} = k_{capture} \exp(-E_a/RT)$$

where E_a is the apparent Arrhenius activation energy. Table 3 includes values for E_a determined using this equation. Such an approach of course represents a gross oversimplification as a model for including 'chemical' effects in ion–molecule reactions since there are reasons other than an activation energy which can cause a low reaction efficiency. Further insight into these reasons must await measurements of the temperature dependence of the rate constants and detailed calculations of reaction surfaces.

Acknowledgments

The financial assistance of the National Research Council of Canada and the Sloan Foundation is gratefully acknowledged.

1. J. L. Franklin (*Editor*). Ion-molecule reactions. Plenum Press, New York. 1972.
2. J. I. Brauman and L. K. Blair. J. Am. Chem. Soc. **91**, 2126 (1969); **93**, 3911 (1971).
3. W. J. Hehre and J. A. Pople. Tetrahedron Lett. 2959 (1970).
4. L. Radom. Aust. J. Chem. **28**, 1 (1975).
5. A. C. Hopkinson, N. K. Holbrook, K. Yates, and I. G. Csizmadia. J. Chem. Phys. **49**, 3596 (1968).
6. D. K. Bohme, R. S. Hemsworth, H. W. Rundle, and H. I. Schiff. J. Chem. Phys. **58**, 3504 (1973).
7. H. S. Johnston. Gas phase reaction rate theory. The Ronald Press Company, New York. 1966.
8. D. K. Bohme, R. S. Hemsworth, and H. W. Rundle. J. Chem. Phys. **59**, 77 (1973).
9. N. C. Barford. Experimental measurements: precision, error and truth. Addison-Wesley, London. 1967.
10. D. Betowski, J. D. Payzant, G. I. Mackay, and D. K. Bohme. Chem. Phys. Lett. **31**, 321 (1975).
11. D. Betowski, G. Mackay, J. Payzant, and D. Bohme. Can. J. Chem. **53**, 2365 (1975).
12. JANAF Thermochemical tables. 2nd ed. Natl. Stand. Ref. Data Ser. Natl. Bur. Stand. **37** (1971).
13. S. W. Benson, F. R. Cruickshank, D. M. Golden, G. R. Haugen, H. E. O'Neal, A. S. Rodgers, R. Shaw, and R. Walsh. Chem. Rev. **69**, 279 (1969).
14. J. I. Brauman and L. K. Blair. J. Am. Chem. Soc. **92**, 5986 (1970).
15. R. Yamdagni and P. Kebarle. J. Am. Chem. Soc. **95**, 4050 (1973).
16. J. I. Brauman and L. K. Blair. J. Am. Chem. Soc. **93**, 4315 (1971).
17. R. T. McIver, Jr. and J. H. Silvers. J. Am. Chem. Soc. **95**, 8462 (1973).
18. D. K. Sen Sharma and J. L. Franklin. J. Am. Chem. Soc. **95**, 6562 (1973).
19. D. K. Bohme. The kinetics and energetics of proton transfer. *In* Interactions between ions and molecules. *Edited by* P. Ausloos. Plenum Press, New York. 1975.
20. T. Su and M. T. Bowers. J. Chem. Phys. **58**, 3027 (1973).
21. T. Su and M. T. Bowers. Int. J. Mass Spectrom. Ion Phys. **12**, 347 (1973).
22. E. W. Roth and R. B. Bernstein. J. Chem. Phys. **31**, 1619 (1959).
23. R. D. Nelson, D. R. Lide, and A. A. Marjott. Natl. Stand. Ref. Data Ser. Nat. Bur. Stand. **10** (1966).
24. J. O. Hirshfelder, C. F. Curtiss, and R. B. Bird. Molecular theory of gases and liquids. John Wiley and Sons, New York. 1967.
25. H. I. Schiff and D. K. Bohme. Int. J. Mass Spectrom. Ion Phys. **16**, 167 (1975).